The hansenula polymorpha pex23 family: overlooked proteins In organelle formation

Wu, Fei

DOI:
10.33612/diss.157801525

CHAPTER 4

The absence of *Hansenula polymorpha* Pex23 and Pex29 affects mitochondrial morphology

Fei Wu, Rinse de Boer, Arjen M. Krikken and Ida J. van der Klei

Molecular Cell Biology, Groningen Biomolecular Sciences and Biotechnology Institute, University of Groningen, 9300CC Groningen, The Netherlands

Abstract

In the yeast *Hansenula polymorpha* all four Pex23 family proteins, Pex23, Pex24, Pex29 and Pex32 localize to the ER. Deletion of *PEX24* or *PEX32* results in major defects in peroxisome biogenesis and function. Deletion of *PEX23* results in weaker peroxisome defects, while in cells lacking *PEX29* peroxisomes are normal. Here, we studied whether the absence of Pex23 family proteins affects other cell organelles in *H. polymorpha*.

Using fluorescence microscopy, less BODIPY 493/503-stained lipid droplets were detected in *pex23* and *pex29* cells compared to the other two deletion mutants and the wild-type control. Upon staining with Mitotracker, we observed altered mitochondrial morphology in the same two mutants. Using FM4-64 no alterations in vacuole morphology could be detected in any of the mutant strains.

Electron microscopy showed that *pex23* and *pex29* cells contain more mitochondria, which are strongly clustered, suggesting that mitochondrial fusion is defective. Localization studies revealed that Pex23 localizes to the peripheral ER and nuclear envelope. At the nuclear envelope Pex23 accumulates at nucleus vacuole junctions, while at the peripheral ER Pex23 is evenly distributed. ER-mitochondria contact sites were still observed in *pex23* cells.

Summarizing, our data indicate that the absence of proteins of the Pex23 family can not only affect peroxisomes and LDs, but also mitochondria.

Keywords: Pex23, Pex29, lipid droplets, mitochondria, yeast

Introduction

Peroxisomes are organelles that contain a proteinaceous matrix and are enclosed by a single membrane. These organelles are dynamic and continuously adjust their number, size and enzyme composition in response to internal and environmental stimuli (Smith and Aitchison, 2013). So far, 37 peroxins have been identified. Peroxins are proteins involved in peroxisome biology and are encoded by *PEX* genes.

Most peroxins localize to the peroxisomal membrane, but receptors for newly synthesized peroxisomal membrane and matrix proteins are cytosolic. Peroxins of the Pex23 protein family localize to the endoplasmic reticulum (ER). This protein family only exist in fungi. Proteins of this family are involved in regulating peroxisome proliferation (Yuan et al., 2016). The number of Pex23 family members and their role in regulating peroxisome abundance and size differ among yeast species. All Pex23 proteins contain a DysF motif at the C-terminus (Kiel et al., 2006). The DysF domain is responsible for adjusting peroxisome number and size in *Pichia pastoris* Pex30 and Pex31 (Yan et al., 2008). In *Hansenula polymorpha*, the DysF domain is not essential for Pex32 function, but needed for accumulation of the protein at peroxisome-ER contact sites (This thesis, Chapter III). The function of the DysF domain in other Pex23 family proteins is still unknown. In the N-terminal domain of Pex23 family proteins one or multiple transmembrane (TM) helixes are predicted (Joshi et al.,

2016; Wu et al., 2020; Yan et al., 2008). The TMs of *H. polymorpha* Pex32 are responsible for sorting to the ER and controlling peroxisome abundance (This thesis, Chapter III). In *Saccharomyces cerevisiae* Pex30 and Pex31 a reticulon-like domain (RHD) is predicted. Importantly, overproduction of this domain of ScPex30 could restore ER structure in cells lacking reticulons, suggesting this domain functions in ER-shaping (Joshi et al., 2016).

The most prevailing model in describing how Pex23 family proteins regulate peroxisome biogenesis is based on studies in *S. cerevisiae*, in which Pex29, Pex30 and Pex31 are in a complex together with the ER reticulon-like proteins Rtn1, Rtn2 and Yop1 at ER-peroxisome contact sites. This protein complex defines the region where pre-peroxisomal vesicles (PPVs) bud off (David et al., 2013; Farré et al., 2019). Deletion of *S. cerevisiae PEX30* and *PEX31* results in a change in both the speed of PPV formation and PPV morphology, which influences peroxisome biogenesis (David et al., 2013; Joshi et al., 2016; Mast et al., 2016).

Recently it was reported that *S. cerevisiae* Pex30 is also involved in regulating lipid droplets (LDs) biogenesis from the ER. Upon deletion of *PEX30,* cells produced more and smaller, clustered LDs (Choudhary et al., 2020; Joshi et al., 2018; Wang et al., 2018). Also, it has been proposed that Pex30, together with other LD biogenesis factors (Yft2, Erg6 and Pet10) are recruited to a seipin defined ER subdomain to initiate nascent LD formation (Choudhary et al., 2020).

Our studies in *H. polymorpha* showed that deletion of *PEX24* or *PEX32* results in severe peroxisome defects. These defects could be suppressed by introducing an artificial ER-peroxisome linker protein, suggesting that Pex24 and Pex32 are important for the formation of peroxisome-ER contacts. In contrast, cells lacking Pex29 showed no peroxisome phenotype, while a slight peroxisome biogenesis defect happened in *pex23* cells. However, the ER-peroxisome artificial linker was unable to rescue this defect.

While HpPex24 and HpPex32 accumulate at peroxisome-ER contact sites, HpPex23 and HpPex29 localize to multiple regions of the ER. In addition, we observed that Pex23 accumulates at nuclear envelope-vacuole junctions (NVJs) (Wu et al., 2020), indicating these proteins are not limited to the ER-peroxisome contact sites. Based on these observations, we want to know whether Pex23 family proteins are also involved in associating ER to other organelles and play a role in regulating the biogenesis of other organelles than peroxisomes.

Here we studied the morphology of other cell organelles in *H. polymorpha* mutant strains lacking one of the Pex23 family members. We show that less BODIPY 493/503-stained LDs could be detected in *H. polymorpha pex23* and *pex29* mutants. In addition, more and clustered mitochondria occur in these two deletion strains compared to *pex24*, *pex32* and wild-type control cells. Vacuole morphology was normal in all four single deletion strains. Detailed localization studies confirmed that Pex23 accumulates at NVJs, but not at ER-mitochondria contact sites. Our data imply that Pex23 family proteins are not only important for peroxisomes and may not all be true peroxins.

Results

Mitochondria and LDs are altered in *pex23* and *pex29* cells

To study whether the absence of Pex23 family proteins from *H. polymorpha* also affects other organelles, we analyzed the vacuoles, LDs and mitochondria in *pex23*, *pex24*, *pex29* and *pex32* cells. Fluorescence microscopy (FM) revealed that in all four mutants FM4-64 marked vacuoles are similar as in WT control cells (Fig. 1). In contrast, upon staining the cells with BODIPY 493/503 much less bright fluorescent spots were observed in *pex23* and *pex29* cells compared to *pex24*, *pex32* and WT controls, indicating that either the number of LDs decreased or their lipid composition changed (Fig. 1). Interestingly, *pex23* and *pex29* deletion strains also displayed aberrant mitochondrial profiles, based on FM analysis of Mitotracker-stained cells. In contrast, in *pex24* and *pex32* cells mitochondrial morphology was similar to what was observed in the WT (Fig. 1). Summarizing, these data show that deletion of *PEX23* or *PEX29* affects LDs and mitochondria, but not vacuoles.

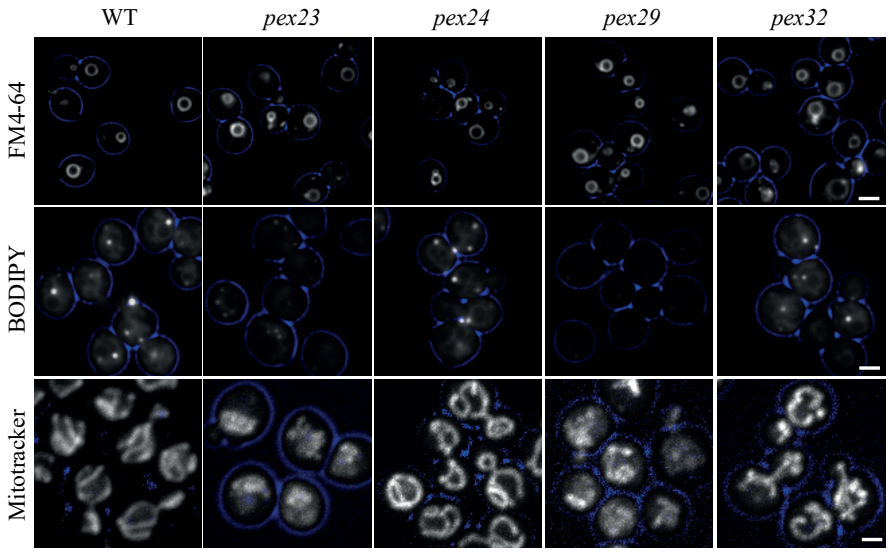

Figure 1. Deletion of *PEX23* or *PEX29* alters mitochondria and LDs. FM images (vacuoles and LDs) and Confocal Laser Scanning Microscopy (CLSM) images (mitochondria) of glucose-grown cells of the indicated deletion strains. Cells were stained with FM4-64 to visualize vacuoles, BODIPY 493/503 for LDs or Mitotracker Orange for mitochondria. Scale bars: 2 μm in FM images, 1 μm in CLSM images.

Mitochondria cluster in *pex23* and *pex29* cells

Next, we performed electron microscopy (EM) to better understand the alterations in mitochondrial morphology. As shown in Fig. 2A, mitochondrial profiles were present throughout the cells in WT, *pex24* and *pex32* cells, in line with the FM observations.

However, in cells lacking Pex23 or Pex29 mitochondrial profiles were highly clustered (Fig. 2A). The number of mitochondrial profiles was quantified in thin sections using EM. This showed that sections of WT cells contained up to 4 mitochondrial profiles, but most sections contained 1 to 3 mitochondrial profiles. A very similar distribution was observed in sections of *pex24* cells. However, in sections of *pex23* and *pex29* cells, and to a lesser extend of *pex32* cells, often 6 or more profiles were observed (Fig. 2A). The absence of Pex23 family members did not lead to an increase in mitochondrial surface area (Fig. 2B).

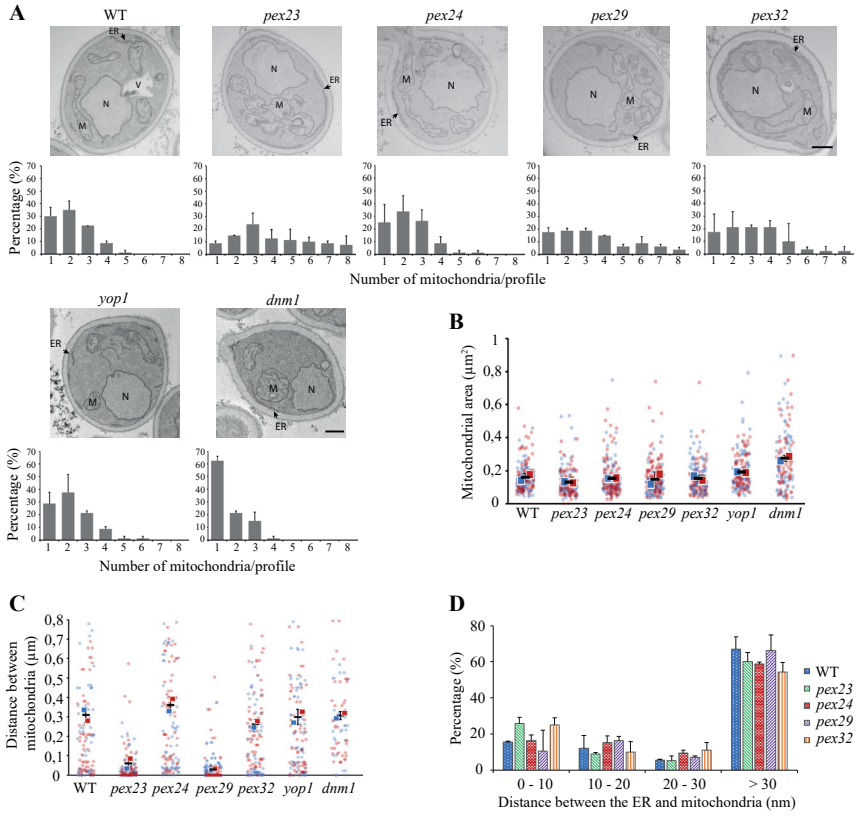

Figure 2. Mitochondria in *pex23* and *pex29* cells are close associated. (A) Electron microscopy (EM) images of thin sections of $KMnO_4$-fixed glucose-grown cells of the indicated strains, and the number of mitochondria per profile have been quantified. Data are mean±s.d. of two independent experiments (n=2 using 40 random sections from each experiment). ER - endoplasmic reticulum; M - mitochondrion; N - nucleus; V - vacuole. Scale bar: 500 nm. (B) Quantification of average mitochondrial area based on EM images of indicated strains. (C) Quantification of the distance between mitochondria in indicated cells. (D) Quantification of the distance between the ER and mitochondrial membranes in the indicated strains. Data are mean±s.d. of two independent experiments. (n=2 using 40 random sections from each experiment).

In thin sections, the percentage of mitochondria that are closely associated with the ER

(distance between both membranes < 30 nm) is similar in all four mutant strains and the WT control. This indicates that in the absence of Pex23 family proteins ER-mitochondria contact sites still occur, like in WT cells (Fig. 2D). Quantification of the distance between mitochondrial profiles confirmed that mitochondria are more clustered in *pex23* and *pex29* mutants, relative to *pex24*, *pex32* and WT controls (Fig. 2C). Further EM analysis of *pex23* cells using serial sections confirmed that these cells contain multiple mitochondria that are clustered (Fig. 3). This analysis also showed that NVJs still occur in *pex23* cells.

We next analyzed cells of a *dnm1* mutant to test whether the alterations in mitochondrial profiles and their clustering were caused by a defect in mitochondrial fission (Bleazard et al., 1999). As shown in Fig. 2A, mitochondrial morphology in *dnm1* cells was very different in comparison to the WT and mutants lacking a Pex23 family protein, because *dnm1* cells contained a single mitochondrial profile. Also, the mitochondrial surface area increased in *dnm1* cells relative to all other strains under study (Fig. 2B).

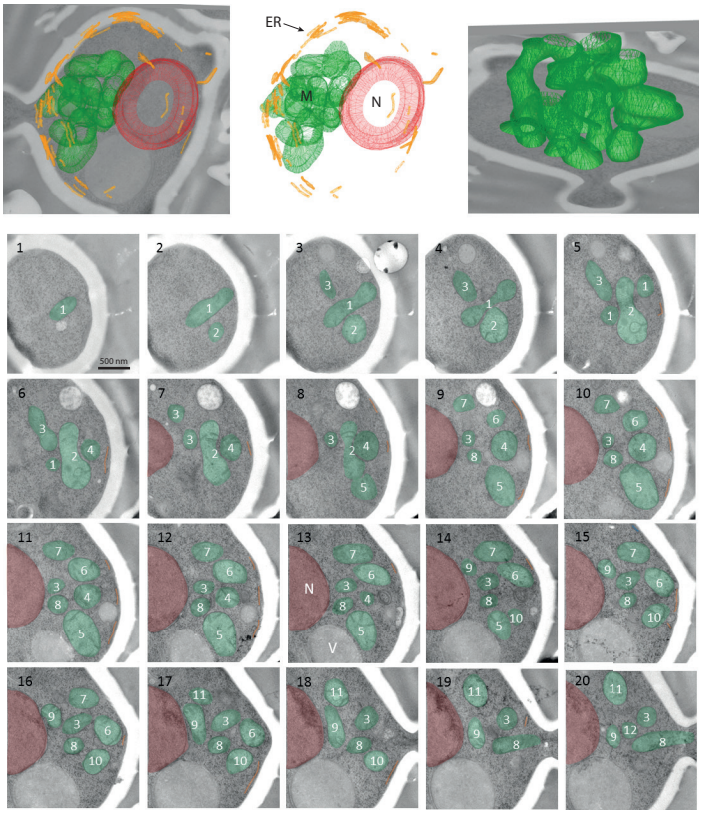

Figure 3. *H. polymorpha pex23* cells contain a cluster of multiple mitochondria. Top: 3D reconstructions of serial sections shown below. Bottom: 20 consecutive sections from a series of serial sections through a glucose-grown *pex23* cell. M - mitochondria (green and numbered), ER- endoplasmic reticulum, N - nucleus (red), V - vacuole.

In *S. cerevisiae* proteins of the Pex23 family have membrane shaping properties and occur in the same complex as reticulons, Rtn1 and Rtn2. *S. cerevisiae* Yop1 is also a reticulon interaction protein that localizes to the ER and plays a role in membrane shaping (Voeltz et al., 2006). Therefore, we asked whether the absence of the *H. polymorpha* homolog of *S. cerevisiae* Yop1 also affects mitochondrial morphology. This was not the case because the number of mitochondrial profiles and the clustering was similar in *H. polymorpha yop1* and WT cells.

Pex23 is present at the peripheral ER and concentrates in NVJs at the nuclear envelope

We previous showed that GFP-tagged Pex23 localizes in multiple spots at the ER also including peroxisome-ER contact sites and NVJs, suggesting that Pex23 is a general contact site protein (Wu et al., 2020). Contact sites between the ER and mitochondria regulate mitochondrial fission and fusion in *S. cerevisiae* (Abrisch et al., 2020; Prinz et al., 2020). If Pex23 plays a role in ER-mitochondrial contacts, this may explain the altered mitochondrial phenotype. Correlative light and electron microscopy (CLEM) was performed to analyze whether Pex23-GFP accumulates at ER-mitochondria contact sites as well. To obtain sufficient fluorescence for CLEM, Pex23-GFP was overproduced using the strong and inducible P_{AOX} promoter (Fig. 4B) In glycerol-grown cells, Pex23-GFP was evenly distributed over the peripheral ER (Fig. 4A). At the nuclear envelope Pex23-GFP accumulated at NVJs. The most intense fluorescent spots were selected for tomography. In most cases these spots occurred at regions were peripheral ER is present (see arrowhead in Fig. 4A). Pex23-GFP did not accumulate in specific patches on the peripheral ER. Therefore, enrichment at ER-mitochondria contact sites likely does not occur.

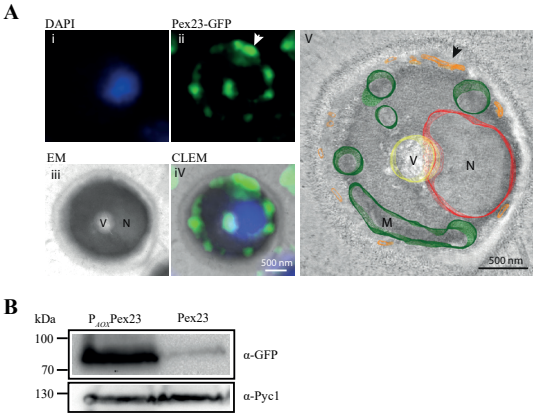

Figure 4. Pex23 localizes at the peripheral and nuclear ER, including NVJs. (A) Correlative Light and Electron Microscopy (CLEM) of cells producing Pex23-GFP under control of the P_{AOX} Nucleus is stained with 4′,6-diamidino-2-phenylindole (DAPI). The arrowhead indicates the most intense GFP spot in the GFP image and the corresponding position in the rendered volume. Cells were induced for 1.5 h on glycerol. V - vacuole, N - nucleus, M - mitochondrion. (B) Western blot analysis of Pex23-GFP levels in the indicated strains grown for 1.5 h on glycerol. Blots were decorated with α-GFP or α-Pyc1 antibodies (loading control).

pex23 cells grow like WT controls on various carbons sources.

H. polymorpha mutants lacking Pex23 family proteins are capable to grow on glucose. *H. polymorpha pex24* and *pex32* cells show a severe growth defect on methanol, in line with the peroxisome biogenesis defect of these cells. Cells lacking Pex29 grow normal on methanol, while growth of *pex23* cells on methanol is reduced (Wu et al., 2020). To test whether *pex23* cells showed any other growth defect, we analyzed the capacity of the cells to grow on carbon sources that are not metabolized by peroxisomal enzymes. As shown in Fig. 5, *pex23* cells grew like WT controls on glycerol and ethanol (Fig. 5).

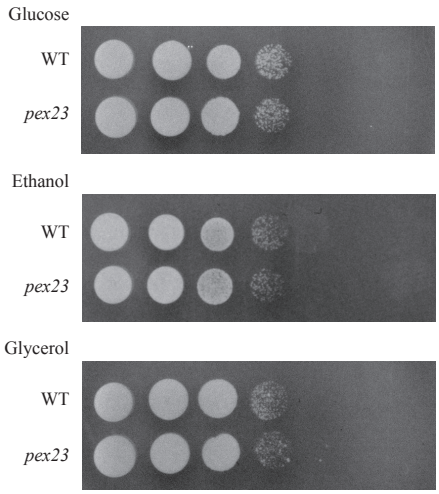

Figure 5. Growth analysis of *pex23* cells. Spot assay analysis of growth of WT and *pex23* cells on mineral medium containing glucose, ethanol or glycerol.

Discussion

In this study, we show for the first time that the absence of a Pex23 family protein can lead to alterations in mitochondrial morphology. Our data indicate that in the yeast *H. polymorpha* deletion of *PEX23* or *PEX29* leads to aberrant mitochondrial morphology together with changes in LDs. The latter is in line with previous findings in *S. cerevisiae pex30* cells, which contain less and smaller LDs (Joshi et al., 2018; Wang et al., 2018). ScPex30 was demonstrated to define the ER subdomain that is involved in LD and PPV formation (Choudhary et al., 2020; Joshi et al., 2018; Wang et al., 2018).

The altered mitochondrial morphology in *H. polymorpha pex23* and *pex29* cells is not indirectly due to peroxisome biogenesis defects, because *pex24* and *pex32* cells are more severely affected in peroxisome formation, but have normal mitochondria (Wu et al., 2020). Conversely, while peroxisomes are normal in *pex29* cells, these cells show clear mitochondrial morphology alterations. The mitochondrial abnormalities of *pex23* and *pex29* cells differ from

that observed in *dnm1* cells, in which mitochondrial fission is blocked. Thus, *pex23* and *pex29* are not defective in mitochondrial fission. The absence of *H. polymorpha* Yop1, an ER protein with membrane shaping properties, had no effect on mitochondria. Detailed comparison of ER morphology in *pex23*, *pex29*, *yop1* and other mutants lacking RHD proteins is required to determine whether ER shape is important for mitochondrial morphology.

We speculate that deletion of *PEX23* or *PEX29* affects mitochondrial fusion. EM analysis of *pex23* cells revealed enhanced numbers of mitochondria that are highly clustered. Hence, these organelles apparently still can divide, but may not be capable to fuse. Indeed, in *S. cerevisiae* a block in mitochondria fusion, caused by the absence of Fzo1, results in fragmented mitochondrial structures that form a cluster in one area of the cell (Hermann et al., 1998). This phenotype is similar to what we observed in *H. polymorpha pex23* and *pex29* cells. However, because Pex23 and Pex29 are ER-resident proteins their role in regulating mitochondrial fusion most likely is indirect and different from Fzo1.

Interestingly, the mitochondrial fusion protein Fzo1 has been identified as tethering protein at mitochondria-peroxisome contact sites in *S. cerevisiae* (Shai et al., 2018). Moreover, upon overproduction Fzo1 also localizes to peroxisomes. Possibly, Fzo1 is involved in multiple contact sites by interacting with different organellar proteins, including Pex23 and Pex29. If so, deletion of *PEX23* or *PEX29* may eliminate this interaction and further affects Fzo1-dependent mitochondrial fusion.

Mitochondrial fusion highly depends on a proper membrane lipid composition (Moon and Jun, 2020). Therefore, the mitochondrial defects in *pex23* and *pex29* cells might be caused by an altered membrane lipid composition. The LD defects in *pex23* and *pex29* mutants support this possibility. Lipid exchange occurs between the ER and mitochondria (Vid and Günther, 2013). Deletion of *PEX23* or *PEX29* may alter this process and affect both ER and mitochondrial membrane lipid composition.

The mitochondrial phenotype of *pex23* and *pex29* cells could also be the result of alterations in ER-mitochondrial contact sites as mitochondrial fission and fusion can occur at these sites (Abrisch et al., 2020). Our EM analysis revealed that ER-mitochondria contacts still occur in *pex23* and *pex29* cells. Although Pex23 does not accumulate at ER-mitochondria contacts, it is present all over the peripheral ER and hence likely also at regions where the ER associates with mitochondria. Importantly, Pex23 does accumulate at NVJs. However, also NVJs are still formed in cells lacking Pex23.

In *S. cerevisiae*, Mmm1, Mdm10, Mdm12 and Mdm34 are the main protein components at ER-mitochondria contact sites (ERMES). This ER-mitochondria contact site is involved in phospholipid transport between both organelles (Kawano et al., 2018). We observed no significant increase in distance between the ER and mitochondrial membrane in cells lacking Pex23. However, this does not exclude the possibility that Pex23 is involved in forming an ER-mitochondria contact site, which plays a role in regulating mitochondrial fission and fusion. If so, deletion of *PEX23* may affect the function of this contact site, explaining why mitochondrial dynamics is disturbed.

Summarizing, our data show for the first time that in *H. polymorpha* deletion of *PEX23* or *PEX29* results in mitochondrial defects, namely in clustering of multiple organelles. These data indicate that proteins of the Pex23 family are not only playing a role in peroxisome biogenesis.

Materials and methods

Strains and growth conditions

H. polymorpha cells were grown in batch culture at 37 °C on mineral media (Van Dijken et al., 1976) supplemented with 0.5% glucose, or 0.25% glycerol for overproducing Pex23 as carbon source. Leucine, when required, was added to a final concentration of 60 μg/ml. For growth on plates, YPD media (1% yeast extract, 1% peptone and 1% glucose) were supplemented with 2% agar. Resistant transformants were selected using 100 μg/ml nourseothricin (WERNER BioAgents) or 300 μg/ml hygromycin (Invitrogen).

The *Escherichia coli* strain DH5α used for cloning. *E. coli* cells were grown at 37 °C in Luria broth (LB) media (1% Bactotryptone, 0.5% Yeast Extract and 0.5% NaCl) supplemented with 100 μg/ml Ampicillin or 50 μg/ml kanamycin. 2% agar was added in LB medium when growing on plates.

Construction of *H. polymorpha* strains

The strains, plasmids and primers used in this study are listed in Table 1, 2 and 3 respectively. Plasmid integration was performed as described previously (Faber et al., 1994). All integrations were confirmed by PCR. Deletion constructions were confirmed by PCR and Southern blotting.

Construction of *yop1* and *dnm1* single deletion strains

The *yop1* deletion strain was constructed by replacing the *YOP1* region with the nourseothricin resistance gene as follows: First, a PCR fragments comprising the nourseothricin resistance gene and 50 bp of the *YOP1* flanking regions were amplified with primers dyop1-F and dyop1-R using plasmid pHIPN4 as a template. The resulting *YOP1* deletion cassette was transformed into *yku80* cells to obtain *yop1* deletion mutant.

To construct *dnm1* strain, a PCR fragment containing *DNM1* deletion cassette was amplified with primers Hyg-Fw01 and Hyg-Rev02 using plasmid pARM001 as a template and then transformed into *yku80* cells resulting in *dnm1* mutant.

Construction of P_{AOX}Pex23-GFP::DsRed-SKL

To construct P_{AOX}Pex23-GFP::DsRed-SKL, first P_{AOX}Pex23-GFP has been constructed. For this strain, a PCR fragment containing *PEX23*-GFP sequence was amplified with primers Pex23-F and Pex23-R using strain Pex23-GFP as a template. The obtained PCR product was digested with *Hin*dIII and *Sal*I, and inserted between the *Hin*dIII and *Sal*I sites of pHIPH4

plasmid, resulting in plasmid pHIPH4-*PEX23*-GFP. *Pfl*mI-linearized pHIPH4-*PEX23*-GFP was transformed into *yku*80 to express P_{AOX}Pex23-GFP.

*Nsi*I-linearized pHIPN4-DsRed-SKL was integrated into P_{AOX}Pex23-GFP to produce DsRed-SKL.

Preparation of yeast TCA lysates

Cell extracts of TCA-treated cells were prepared for SDS-PAGE as described previously (Baerends et al., 2000). Equal amounts of protein were loaded per lane and blots were probed with anti-mGFP antibodies (sc-9996, Santa Cruz Biotech; 1:2000 dilution), or anti-pyruvate carboxylase 1 (Pyc1) antibodies (Ozimek et al., 2007; 1:10,000 dilution). Secondary goat anti-rabbit (31460) or goat anti-mouse (31430) antibodies conjugated to horseradish peroxidase (HRP) (Thermo Scientific; 1:5000 dilution) were used for detection. Pyc1 was used as a loading control. Blots were scanned using a densitometer (Bio-Rad, GS-710).

Spot assay

Exponential glucose growing cells were harvested by centrifugation and diluted to an OD_{600} of 1.0 in water. Serial dilutions of were made (10^{-1}, 10^{-2}, 10^{-3}, 10^{-4}, 10^{-5}) and spotted on mineral medium plates containing glucose (0.5%), glycerol (0.25%) or ethanol (0.25%). These plates were incubated for 48 h at 37 °C.

Fluorescence microscopy

Images were obtained from the cells in growth media or on 200 nm thick cryosections for CLEM using a fluorescence microscope (Axioscope A1; Carl Zeiss) using Micro-Manager software and a digital camera (Coolsnap HQ^2; Photometrics). The GFP and BODIPY fluorescence were visualized with a 470/40 nm band-pass excitation filter, a 495 nm dichromatic mirror, and a 525/50 nm band-pass emission filter. Mitotracker and FM4-64 fluorescence were visualized with a 546/12 nm band-pass excitation filter, a 560 nm dichromatic mirror, and a 575-640 nm band-pass emission filter. DAPI fluorescence was visualized with a 380/30 nm band-pass excitation filter, a 420 nm dichromatic mirror, and a 460/50 nm band-pass emission.

For vacuolar staining, 1 ml of cell culture was supplemented with 1 µl FM4-64 (Invitrogen), incubated for 60 min at 37°C, and analyzed. The lipid droplet dye BODIPY 493/503 (Invitrogen) was used at a concentration of 1 µg/ml, incubated for 10 min at 37°C. Mitochondria were stained by adding 0.1 µl Mitotracker Orange (1 mM) to 1 ml of cells. These cells were incubated for 5 min at 37 °C and subsequently spotted on agar containing glucose.

Image analysis was performed using ImageJ, and figures were prepared using Adobe Illustrator software.

Electron microscopy

For morphological analysis, cells were fixed in 1.5% potassium permanganate, post-stained with 0.5% uranyl acetate and embedded in Epon. Mitochondrial area, distances between mitochondria, and distance between the ER and mitochondria are measured in ImageJ.

Serial sectioning was performed on cryo-fixed cells. For this cells are cryo-fixed and freeze substituted as described previously (Wu et al., 2018). 60 nm serial sections are collected on formfar coated single slot copper grids and inspected with a CM12 TEM (Philips).

Correlative light and electron microscopy (CLEM) was performed as described previously (Knoops et al., 2015). After fluorescence imaging, the grid was post-stained and embedded in a mixture of 0.5% uranyl acetate and 0.5% methylcellulose. Acquisition of the double-tilt tomography series was performed manually in a CM12 TEM (Philips) running at 100 kV, and included a tilt range of 45° to −45° with 2.5° increments. To construct the CLEM images, pictures taken with FM and EM were aligned using the eC-CLEM plugin in Icy (Paul-Gilloteaux et al., 2017) (http://icy.bioimageanalysis.org). Reconstruction of the tomograms and alignment of the serial sections was performed using the IMOD software package (https://bio3d.colorado.edu/imod/).

Funding

This work was supported by a grant from the China Scholarship Council (CSC) to F.W.

References

Abrisch, R. G., Gumbin, S. C., Wisniewski, B. T., Lackner, L. L. and Voeltz, G. K. (2020). Fission and fusion machineries converge at ER contact sites to regulate mitochondrial morphology. *J. Cell Biol*. **219**. doi:10.1083/jcb.201911122

Baerends, R. J. S., Faber, K. N., Kram, A. M., Kiel, J. A. K. W., van der Klei, I. J., and Veenhuis, M. (2000). A stretch of positively charged amino acids at the N terminals of Hansenula polymorpha Pex3p is involved in incorporation of the protein into the peroxisomal membrane. *J. Biol. Chem*. **275**, 9986–9995. doi:10.1074/jbc.275.14.9986

Bleazard, W., McCaffery, J. M., King, E. J., Bale, S., Mozdy, A., Tieu, Q., Nunnari, J. and Shaw, J. M. (1999). The dynamin-related GTPase Dnm1 regulates mitochondrial fission in yeast. *Nat. Cell Biol*. **1**, 298–304. doi:10.1038/13014

Cepińska, M. N., Veenhuis, M., van der Klei, I. J. and Nagotu, S. (2011). Peroxisome fission is associated with reorganization of specific membrane proteins. *Traffic* **12**, 925–937. doi:10.1111/j.1600-0854.2011.01198.x

Choudhary, V., El Atab, O., Mizzon, G., Prinz, W. A. and Schneiter, R. (2020). Seipin and Nem1 establish discrete ER subdomains to initiate yeast lipid droplet biogenesis. *J. Cell Biol*. **219**, 218–221. doi:10.1083/jcb.201910177

David, C., Koch, J., Oeljeklaus, S., Laernsack, A., Melchior, S., Wiese, S., Schummer, A., Erdmann, R., Warscheid, B. and Brocard, C. (2013). A combined approach of quantitative interaction proteomics and live-cell imaging reveals a regulatory role for endoplasmic reticulum (ER) reticulon homology proteins in peroxisome biogenesis. *Mol. Cell. Proteomics* **12**, 2408–2425. doi:10.1074/mcp.M112.017830

Faber, K. N., Haima, P., Harder, W., Veenhuis, M. and Ab, G. (1994). Highly-efficient electrotransformation of the yeast Hansenula polymorpha. *Curr. Genet*. **25**, 305–310. doi:10.1007/BF00351482

Farré, J., Mahalingam, S. S., Proietto, M. and Subramani, S. (2019). Peroxisome biogenesis, membrane contact sites, and quality control. *EMBO Rep.* **20**, e46864. doi:10.15252/embr.201846864

Hermann, G. J., Thatcher, J. W., Mills, J. P., Hales, K. G., Fuller, M. T., Nunnari, J. and Shaw, J. M. (1998). Mitochondrial fusion in yeast requires the transmembrane GTPase Fzo1p. *J. Cell Biol*. **143**, 359–373. doi:10.1083/jcb.143.2.359

Joshi, A. S., Huang, X., Choudhary, V., Levine, T. P., Hu, J. and Prinz, W. A. (2016). A family of membrane-shaping proteins at ER subdomains regulates pre-peroxisomal vesicle biogenesis. *J. Cell Biol*. **215**, 515–529. doi:10.1083/jcb.201602064

Joshi, A. S., Nebenfuehr, B., Choudhary, V., Satpute-Krishnan, P., Levine, T. P., Golden, A. and Prinz, W. A. (2018). Lipid droplet and peroxisome biogenesis occur at the same ER subdomains. *Nat. Commun*. **9**, 2940. doi:10.1038/s41467-018-05277-3

Kiel, J. A. K. W., Veenhuis, M. and van der Klei, I. J. (2006). PEX genes in fungal genomes: Common, rare or redundant. *Traffic* **7**, 1291–1303. doi:10.1111/j.1600-0854.2006.00479.x

Knoops, K., de Boer, R., Kram, A. and Van Der Klei, I. J. (2015). Yeast pex1 cells contain peroxisomal ghosts that import matrix proteins upon reintroduction of Pex1. *J. Cell Biol*. **211**, 955–962. doi:10.1083/jcb.201506059

Kornmann, B., Currie, E., Collins, S. R., Schuldiner, M., Nunnari, J., Weissman, J. S. and Walter, P. (2009). An ER-mitochondria tethering complex revealed by a synthetic biology screen. *Science* **325**, 477–481. doi:/10.1126/science.1175088

Kumar, S., Singh, R., Williams, C. P. and van der Klei, I. J. (2016). Stress exposure results in increased peroxisomal levels of yeast Pnc1 and Gpd1, which are imported via a piggy-backing mechanism. *Biochim. Biophys. Acta Mol. Cell Res*. **1863**, 148–156. doi:10.1016/j.bbamcr.2015.10.017

Mast, F. D., Jamakhandi, A., Saleem, R. A., Dilworth, D. J., Rogers, R. S., Rachubinski, R. A. and Aitchison, J. D. (2016). Peroxins Pex30 and Pex29 dynamically associate with reticulons to regulate peroxisome biogenesis from the endoplasmic reticulum. *J. Biol. Chem.* **291**, 15408–15427. doi:10.1074/jbc.M116.728154

Moon, Y. and Jun, Y. (2020). The Effects of Regulatory Lipids on Intracellular Membrane Fusion Mediated by Dynamin-Like GTPases. *Front. Cell Dev. Biol.* **8**. doi:10.3389/fcell.2020.00518

Ozimek, P. Z., Klompmaker, S. H., Visser, N., Veenhuis, M. and van der Klei, I. J. (2007). The transcarboxylase domain of pyruvate carboxylase is essential for assembly of the peroxisomal flavoenzyme alcohol oxidase. *FEMS Yeast Res.* **7**, 1082–1092. doi:10.1111/j.1567-1364.2007.00214.x

Paul-Gilloteaux, P., Heiligenstein, X., Belle, M., Domart, M.-C., Larijani, B., Collinson, L., Raposo, G. and Salamero, J. (2017). Erratum: Corrigendum: eC-CLEM: flexible multidimensional registration software for correlative microscopies. *Nat. Methods* **14**, 323–323. doi:10.1038/nmeth0317-323a

Prinz, W. A., Toulmay, A. and Balla, T. (2020). The functional universe of membrane contact sites. *Nat. Rev. Mol. Cell Biol.* **21**, 7–24. doi:10.1038/s41580-019-0180-9

Saraya, R., Krikken, A. M., Kiel, J. A. K. W., Baerends, R. J. S., Veenhuis, M. and van der Klei, I. J. (2012). Novel genetic tools for Hansenula polymorpha. *FEMS Yeast Res.* **12**, 271–278. doi:10.1111/j.1567-1364.2011.00772.x

Shai, N., Yifrach, E., Van Roermund, C. W. T., Cohen, N., Bibi, C., Ijlst, L., Cavellini, L., Meurisse, J., Schuster, R., Zada, L. et al., (2018). Systematic mapping of contact sites reveals tethers and a function for the peroxisome-mitochondria contact. *Nat. Commun.* **9**, 1761 doi:10.1038/s41467-018-03957-8

Smith, J. J. and Aitchison, J. D. (2013). Peroxisomes take shape. *Nat. Rev. Mol. Cell Biol.* **14**, 803–817. doi:10.1038/nrm3700

Van Dijken, L. P., Otto, R. and Harder, W. (1976). Growth of Hansenula polymorpha in a methanol-limited chemostat. *Arch. Microbiol.* **111**, 137–144. doi:10.1007/BF00446560

Vid, V. and Günther, D. (2013). Lipid Transport between the Endoplasmic Reticulum and Mitochondria. *Cold Spring Harb. Perspect. Biol.* **5**. doi:10.1101/cshperspect.a013235

Voeltz, G. K., Prinz, W. A., Shibata, Y., Rist, J. M. and Rapoport, T. A. (2006). A class of membrane proteins shaping the tubular endoplasmic reticulum. *Cell* **124**, 573–586. doi:10.1016/j.cell.2005.11.047

Wang, S., Idrissi, F. Z., Hermansson, M., Grippa, A., Ejsing, C. S. and Carvalho, P. (2018). Seipin and the membrane-shaping protein Pex30 cooperate in organelle budding from the endoplasmic reticulum. *Nat. Commun.* **9**, 1–12. doi:10.1038/s41467-018-05278-2

Wu, F., de Boer, R., Krikken, A. M., Akşit, A., Bordin, N., Devos, D. P. and van der Klei, I. J. (2020). Pex24 and Pex32 are required to tether peroxisomes to the ER for organelle biogenesis, positioning and segregation in yeast. *J. Cell Sci.* **133**. doi:10.1242/jcs.246983

Wu, H., de Boer, R., Krikken, A. M., Akşit, A., Yuan, W. and van der Klei, I. J. (2018). Peroxisome development in yeast is associated with the formation of Pex3-dependent peroxisome-vacuole contact sites. *Biochim. Biophys. Acta Mol. Cell Res.* **1866**, 349–359. doi:10.1016/j.bbamcr.2018.08.021

Yan, M., Rachubinski, D. A., Joshi, S., Rachubinski, R. A. and Subramani, S. (2008). Dysferlin domain-containing proteins, Pex30p and Pex31p, localized to two compartments, control the number and size of Oleate-induced peroxisomes in Pichia pastoris. *Mol. Biol. Cell* **19**, 885–898. doi:10.1091/mbc.e07-10-1042

Yuan, W., Veenhuis, M. and van der Klei, I. J. (2016). The birth of yeast peroxisomes. *Biochim. Biophys. Acta Mol. Cell Res.* **1863**, 902–910. doi:10.1016/j.bbamcr.2015.09.008

Table 1. Strains used in this study

Strain	Characteristics	Reference
yku80	NCYC495 *yku80* deletion strain; *leu 1.1, URA3*	(Saraya et al., 2012)
pex23	*yku80* with *PEX23* deletion strain; *leu 1.1,URA3,* Zeo^R	(Wu et al., 2020)
pex24	*yku80* with *PEX24* deletion strain; *leu 1.1,URA3,* Zeo^R	(Wu et al., 2020)
pex29	*yku80* with *PEX29* deletion strain; *leu 1.1,URA3,* Zeo^R	(Wu et al., 2020)
pex32	*yku80* with *PEX32* deletion strain; *leu 1.1,URA3,* Zeo^R	(Wu et al., 2020)
yop1	*yku80* with *YOP1* deletion strain; *leu 1.1,URA3,* Nat^R	This study
dnm1	*yku80* with DNM1 deletion strain; *leu 1.1,URA3,* Hph^R	This study
Pex23-GFP	*yku80* with pHIPZ-PEX23-mGFP; *leu 1.1,URA3,* Zeo^R	(Wu et al., 2020)
P_{AOX}Pex23-GFP::DsRed-SKL	*Pex23-mGFP* with pHIPN4-DsRed-SKL; *leu 1.1,URA3,* Zeo^R, Nat^R	This study

Table 2. Plasmids used in this study

Plasmid	Description	Reference
pHIPN4	pHIPN plasmid containing *AOX* promoter; Amp^R, Nat^R	(Cepińska et al., 2011)
pARM001	pHIPH plasmid containing the C-terminal of *PEX14* fused to mCherry; Amp^R, Hph^R	(Kumar et al., 2016)
pHIPZ-*PEX23*-GFP	pHIPZ plasmid containing the C-terminal of *PEX23* fused to mGFP; Amp^R, Zeo^R	(Wu et al., 2020)
pHIPH4	Plasmid containing *HPH* marker under the control of *AOX* promoter; Amp^R,Hph^R	(Saraya et al., 2012)
pHIPH4-*PEX23*-GFP	pHIPH plasmid containing *PEX23*-GFP under the control of *AOX* promoter; Amp^R, Hph^R	This study
pHIPN4-DsRed-SKL	pHIPN plasmid containing the DsRed-SKL under the control of *AOX* promoter; Amp^R, Nat^R	(Cepińska et al., 2011)

Table 3. Primers used in this study

Primer	Sequence (5' to 3')
dyop1-F	CATCATGGATTTCAACAAGCTGCAAGCCCAAGTGCAAAACGCGTTTTCTGTAACCCACA-CACCATAGCTTCAAAATG
dyop1-R	CTTCTGCTCTTGCATACCCTTTGCAGTCTTACTGAGTCTTCTCCTGGACCATCATCGAT-GAATTCGAGCTCGTTTTC
Hyg-Fw01	GAATACATTTCCAAGCCAAACTCGATTATTCTAGCTGTTTCTCCAGCCAATAACCCACACAC-CATAGCTTCAA
Hyg-Rev02	ACCGAACCATTTGGCGACCTGGCATGGTCTTTACTCTTCTGTTTCTGTTT CGTTTTCGACACTGGATGGC
Pex23-F	CCCAAGCTTATGCCTACGGATCCGAACTC
Pex23-R	GCAGTCGACTTACTTGTACAGCTCGTCCA